1

Numerical Analysis Techniques

Ramesh Garg
Indian Institute of Technology, Kharagpur, India

1.1 Introduction

Microstrip and other printed antennas are constituted of, in general, patches, strips, slots, packaged semiconductor devices, radome, feed, etc. in a nonhomogeneous dielectric medium. Finite substrate and ground plane size are the norm. The dielectric used is very thin compared to the other dimensions of the antenna. The design of these antennas based on models such as transmission line model or cavity model is approximate. Besides, these designs fit regular-shaped geometries (rectangular, circular, etc.) only, whereas most of the useful antenna geometries are complex and do not conform to these restrictions [1]. The effect of surface waves, mutual coupling, finite ground plane size, anisotropic substrate, etc. is difficult to include in these types of design. The numerical techniques, on the other hand, can be used to analyze any complex antenna geometry including irregular shape, finite dielectric and ground plane size, anisotropic dielectric, radome, etc. The popular numerical techniques for antenna analysis include method of moments (MoM), finite element method (FEM), and finite difference time domain method (FDTD). MoM analysis technique, though efficient, is not versatile because of its dependence on Green's function. FEM and FDTD are the most suitable numerical analysis techniques for printed antennas. FDTD is found to be versatile because any embedded semiconductor device in the antenna can be included in the analysis at the device-field interaction level. This leads to an accurate analysis of active antennas. Maxwell's equations are solved as such in FDTD, without analytical pre-processing, unlike the other numerical techniques. Therefore, almost any antenna geometry can be analyzed. However, this technique is numerically intensive, and therefore require careful programming to reduce computation cost. We shall describe the advances in FDTD. Our reference in this respect is the classic book on FDTD by Taflove and Hagness [2].

A large number of FDTD algorithms have been developed. These can be classified as conditionally stable and unconditionally stable. The conditionally stable schemes include the original or Yee's FDTD also called FDTD (2,2), FDTD (2,4), sampling bi-orthogonal time-domain (SBTD) and their variants; and the unconditionally stable schemes include ADI

Microstrip and Printed Antennas: New Trends, Techniques and Applications. Edited by Debatosh Guha and Yahia M.M. Antar

(Alternate Direction Implicit), CN (Crank Nicolson), CNSS (Crank Nicolson Split Step), LOD (Local One-Dimensional) and their variants. The updating of fields in conditionally stable schemes does not require a solution of matrix equation as an intermediate step, and are therefore fully explicit. However, these schemes have a limit on the maximum value of the time step, which is governed by the minimum value of the space step through the Courant-Friedrich-Levy (CFL) condition.

$$c.\Delta t_{CFL} \leq \frac{1}{\sqrt{1/\Delta x^2+1/\Delta y^2+1/\Delta z^2}} \tag{1.1}$$

Due to the heterogeneous nature of the dielectric in the printed antennas, the wave velocity is less than c and may vary from cell to cell and from one frequency to another. We therefore introduce a safety margin and choose $\Delta t = (1/2)\Delta t_{CFL}$ uniformly to simplify coding and avoid instability. Defining the Courant number q as

$$q = \Delta t/\Delta t_{CFL} \tag{1.2}$$

implies that $q = 1/2$ and the wave takes $2\Delta t$ time to travel to the next node.

The value of Δt_{CFL} puts a severe computational constraint on the structures as they have fine geometrical features such as narrow strips or slots or thin dielectric sheets. Since the simulation time of an antenna is independent of space and time steps, the number of updates of fields increases linearly with the decrease in the time step. This results in an increase in processor time. The limitation on Δt_{CFL} is removed in some of the FDTD algorithms and these are therefore called unconditionally stable schemes. In these schemes one can use the same value of the time step over the whole geometry even if fine geometrical features exist without significantly affecting the accuracy of simulation results. Updating fields in unconditionally stable schemes is carried out in stages called time splitting and involves solving a set of simultaneous equations before going on to the next stage. These schemes therefore are more computationally intensive. However, their accuracy is similar to that of conditionally stable FDTD schemes.

The FDTD analysis of open region problems such as antennas necessitates the truncation of the domain to conserve computer resources. The truncation of the physical domain of the antenna is achieved through absorbing boundary conditions, either analytical ABC or material ABC. Material ABC in the form of PML can achieve a substantial truncation of domain with very low reflection. The design of PML should be compatible with the FDTD scheme employed for the rest of the antenna. A number of PML formulations are available. These are split-field and non split-field PML. Non split-field types are convenient for coding and are therefore preferred. Of the various PML formulations available now, uniaxial PML looks promising.

All the FDTD algorithms suffer from computational error, and the amount of error is related to the space and time step sizes employed. The error is quantified in the form of numerical dispersion. The goal of various FDTD schemes is to analyze multi-wavelength long complex geometries, efficiently and accurately. The complexity of the geometry may be in the form of fine geometrical dimensions, anisotropic dispersive medium, embedded packged semiconductor device, feed, mounting structure, etc. The efficient FDTD algorithms try to achieve this

aim by increasing the permissible space step size without increasing dispersion, by an increase in the time step size compatible with fine geometrical features, the applicability of the algorithm to anisotropic and dispersive medium and reduced reflection from the PML medium. The presence of thin strips/slots makes uniform discretization an inefficient approach. New and efficient solutions are being tested in the form of a sub-cell approach, quasi-static approximation, etc. The treatment of PEC and PMC boundary conditions presented by irregular geometries is receiving due attention, while the interface conditions interior to the device are somewhat difficult to implement accurately. Modeling of fast variation of fields in metal, and analysis of curved geometries is being attempted. We shall now discuss the advances in FDTD analysis since 2003.

Yee's algorithm is outlined first in order to define the grid structure and the placement of electric and magnetic field components on the Yee cell. This grid will be used as a reference for other FDTD algorithms.

1.2 Standard (Yee's) FDTD Method

The FDTD method was first proposed by Yee in 1966 [3] and has been used by many investigators because of its host of advantages. However, computer memory and processing time for FDTD have to be huge to deal with the problems which can be analyzed using techniques based on the analytical pre-processing of Maxwell's equations such as MoM, mode matching, method of lines, FEM, etc. Therefore, the emphasis in the development of FDTD technique is to reduce the requirement for computer resources so that this technique can be used to analyze electrically large complex electromagnetic problems.

To determine time-varying electromagnetic fields in any linear, isotropic media with constants ε, μ, σ Maxwell's curl equations are sufficient; the curl equations are

$$\nabla \times \mathbf{H} = \sigma \mathbf{E} + \varepsilon \frac{\partial \mathbf{E}}{\partial t} \tag{1.3a}$$

$$-\nabla \times \mathbf{E} = \mu \frac{\partial \mathbf{E}}{\partial t} \tag{1.3b}$$

The partial differential equations (1.3) are solved subject to the conditions that: (i) the fields are zero at all nodes in the device at $t = 0$ except at the plane of excitation; (ii) the tangential components of E and H on the boundary of the domain of the antenna must be given for all $t > 0$. For computer implementation of Equation (1.3), the partial derivatives are implemented as finite difference approximations, and are partly responsible for the inaccuracy of the solution. For better accuracy, the central difference approximation is used in FDTD and is defined as,

$$\left.\frac{\partial \mathrm{F}}{\partial \mathrm{u}}\right|_{\mathrm{u_o}} = \left.\frac{\mathrm{F}\left(\mathrm{u_o} + \frac{\Delta \mathrm{u}}{2}\right) - \mathrm{F}\left(\mathrm{u_o} - \frac{\Delta \mathrm{u}}{2}\right)}{\Delta \mathrm{u}}\right|_{\Delta \mathrm{u} \to 0} + \mathrm{O}(\Delta \mathrm{u})^2 \tag{1.4}$$

where $O(\cdot)$ stands for *the order of*. Use of Equation (1.4) converts Equation (1.3) into the following form:

$$E_x^{n+1}(i+\tfrac{1}{2},j,k) = \left(\frac{\varepsilon-\sigma\Delta t/2}{\varepsilon+\sigma\Delta t/2}\right)E_x^n(i+\tfrac{1}{2},j,k) + \frac{\Delta t/\Delta y}{\varepsilon+\sigma\Delta t/2}\left(H_z^{n+1/2}(i+\tfrac{1}{2},j+\tfrac{1}{2},k)-H_z^{n+1/2}(i+\tfrac{1}{2},j-\tfrac{1}{2},k)\right) - \frac{\Delta t/\Delta z}{\varepsilon+\sigma\Delta t/2}\left(H_y^{n+1/2}(i+\tfrac{1}{2},j,k+\tfrac{1}{2})-H_y^{n+1/2}(i+\tfrac{1}{2},j,k-\tfrac{1}{2})\right) \tag{1.5a}$$

$$E_y^{n+1}(i,j+\tfrac{1}{2},k) = \left(\frac{\varepsilon-\sigma\Delta t/2}{\varepsilon+\sigma\Delta t/2}\right)E_y^n(i,j+\tfrac{1}{2},k) + \frac{\Delta t/\Delta z}{\varepsilon+\sigma\Delta t/2}\left(H_x^{n+1/2}(i,j+\tfrac{1}{2},k+\tfrac{1}{2})-H_x^{n+1/2}(i,j+\tfrac{1}{2},k-\tfrac{1}{2})\right) - \frac{\Delta t/\Delta x}{\varepsilon+\sigma\Delta t/2}\left(H_z^{n+1/2}(i+\tfrac{1}{2},j+\tfrac{1}{2},k)-H_z^{n+1/2}(i-\tfrac{1}{2},j+\tfrac{1}{2},k)\right) \tag{1.5b}$$

$$E_z^{n+1}(i,j,k+\tfrac{1}{2}) = \left(\frac{\varepsilon-\sigma\Delta t/2}{\varepsilon+\sigma\Delta t/2}\right)E_z^n\left(i,j,k+\tfrac{1}{2}\right) + \frac{\Delta t/\Delta x}{\varepsilon+\sigma\Delta t/2}\left(H_y^{n+1/2}(i+\tfrac{1}{2},j,k+\tfrac{1}{2})-H_y^{n+1/2}(i-\tfrac{1}{2},j,k+\tfrac{1}{2})\right) - \frac{\Delta t/\Delta y}{\varepsilon+\sigma\Delta t/2}\left(H_x^{n+1/2}(i,j+\tfrac{1}{2},k+\tfrac{1}{2})-H_x^{n+1/2}(i,j-\tfrac{1}{2},k+\tfrac{1}{2})\right) \tag{1.5c}$$

$$H_x^{n+\frac{1}{2}}(i,j+\tfrac{1}{2},k+\tfrac{1}{2}) = H_x^{n-\frac{1}{2}}(i,j+\tfrac{1}{2},k+\tfrac{1}{2}) - \frac{\Delta t}{\mu\Delta y}\left(E_z^n(i,j,k+\tfrac{1}{2})-E_z^n(i,j-1,k+\tfrac{1}{2})\right) + \frac{\Delta t}{\mu\Delta z}\left(E_y^n(i,j+\tfrac{1}{2},k)-E_y^n(i,j+\tfrac{1}{2},k-1)\right) \tag{1.5d}$$

$$H_y^{n+\frac{1}{2}}(i+\tfrac{1}{2},j,k+\tfrac{1}{2}) = H_y^{n-\frac{1}{2}}(i+\tfrac{1}{2},j,k+\tfrac{1}{2}) - \frac{\Delta t}{\mu\Delta z}\left(E_x^n(i+\tfrac{1}{2},j,k)-E_x^n(i+\tfrac{1}{2},j,k-1)\right) + \frac{\Delta t}{\mu\Delta x}\left(E_z^n(i,j,k+\tfrac{1}{2})-E_z^n(i-1,j,k+\tfrac{1}{2})\right) \tag{1.5e}$$

$$H_z^{n+\frac{1}{2}}(i+\tfrac{1}{2},j+\tfrac{1}{2},k) = H_z^{n-\frac{1}{2}}(i+\tfrac{1}{2},j+\tfrac{1}{2},k) - \frac{\Delta t}{\mu\Delta x}\left(E_y^n(i,j+\tfrac{1}{2},k)-E_y^n(i-1,j+\tfrac{1}{2},k)\right) + \frac{\Delta t}{\mu\Delta y}\left(E_x^n(i+\tfrac{1}{2},j,k)-E_x^n(i+\tfrac{1}{2},j-1,k)\right) \tag{1.5f}$$

The indices i, j, and k define the position of the field nodes, such that $x = i\Delta x,\ y = j\Delta y,\ z = k\Delta z$. The time instant is defined by $t = n\Delta t$. To implement the finite difference scheme in three dimensions, the antenna is divided into a number of cells, called Yee cells, of dimension $\Delta x\Delta y\Delta z$. One such cell is shown in Figure 1.1. Remarkably the positions of different components of E and H on the cell satisfy the differential and integral forms of Maxwell's equations. One may note from Figure 1.1 that the placements of the E and H nodes are offset in space by half a space step; it is called staggered grid. We note from Equation (1.5) that the time instants when the E and H field components are calculated are offset by half a time step, that is, components of E are calculated at $n\Delta t$ and components of H are calculated at $(n + 1/2)\Delta t$. The alternate update of E and H fields is called *leap frog* and saves computer processing time.

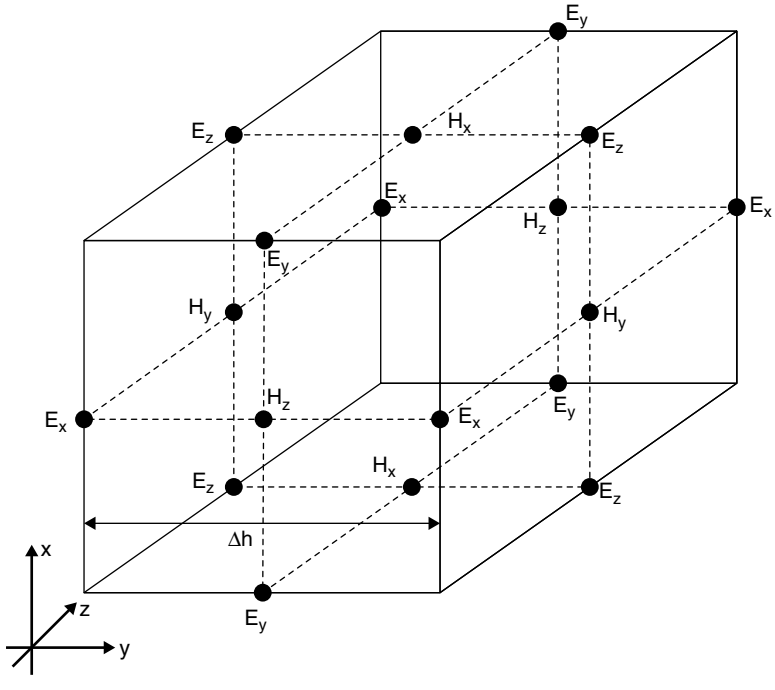

Figure 1.1 Geometry of Yee's cell used in FDTD analysis

1.3 Numerical Dispersion of FDTD and Hybrid Schemes

The finite difference form of derivative (1.4) has an error term $O(\Delta u)^2$. As a result, Equations (1.5 a–f) are second-order accurate, resulting in an approximate solution of the problem. The first sign of this approximation appears in the phase velocity v_{ph} for the numerical wave being different from that in the continuous case. This phenomenon is called numerical dispersion. The amount of dispersion depends on the wavelength, the direction of propagation in the grid, time step Δt and the discretization size Δu. The above algorithm is second-order accurate in space and time, and is therefore called FDTD(2,2). The numerical dispersion for plane wave propagation may be determined from the following expression

$$\left(\frac{\sin(\omega\Delta t/2)}{c\Delta t}\right)^2 = \left(\frac{\sin(\bar{k}\sin\theta\cos\varphi\Delta x/2)}{\Delta x}\right)^2 + \left(\frac{\sin(\bar{k}\sin\theta\sin\varphi\Delta y/2)}{\Delta y}\right)^2 + \left(\frac{\sin(\bar{k}\cos\theta\Delta z/2)}{\Delta z}\right)^2 \tag{1.6}$$

where $\bar{k}$ is the wave number for the numerical wave. The phase velocity $\bar{v} = \omega/\bar{k}$ is determined by solving Equation (1.6) as a function of discretizations $\Delta x, \Delta y, \Delta z, \Delta t$ and propagation angle θ, ϕ. The phase velocity is found to be maximum and close to the velocity of light for propagation along the diagonals and minimum for waves propagating along the axis.

1.3.1 *Effect of Non-Cubic Cells on Numerical Dispersion*

Devices with high aspect ratio may be analyzed by using uniform or non-uniform cell size. An alternative is to employ non-square or non-cubic cells. The influence of the aspect ratio of the unit cell on the numerical dispersion of FDTD(2,2) has been reported by Zhao [4]. It is found that the dispersion error $(c-\bar{v})/c$ increases with the increase in aspect ratio of the cell but reaches an upper limit for aspect ratios greater than 10. For N (number of cells per wavelength, $\lambda/\Delta) = 10$, the maximum dispersion error for non-cubic cells is 1.6% which decreases to 0.4% for N = 20, showing second-order accuracy. In general, the maximum error for non-cubic cells is about 1.5 times that of the corresponding error for cubic cells. For the non-square cells, this ratio is twice that of square cells [4]. For guidance, the minimum mesh resolution required to achieve a desired phase velocity error is plotted in Figure 1.2 for the cubic and non-cubic cells.

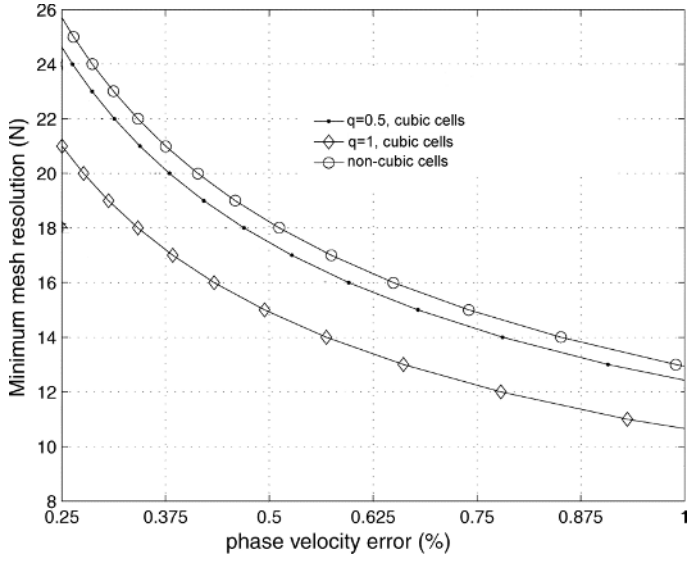

Figure 1.2 Comparison of minimum mesh resolution required for a given accuracy of phase velocity when non-cubic (with high aspect ratio) or cubic unit cells are employed. Reproduced by permission of ©2004 IEEE, Figure 8 of [4]

It may be noted from Figure 1.2 that 0.5% accuracy in phase velocity is achieved for N = 18.5, and N = 13 is needed for 1% accuracy when non-cubic cells are employed. This study shows that unit cells with very high aspect ratio may be used by sacrificing a small amount of accuracy in phase velocity. FDTD(2,2) is also employed for benchmarking other schemes.

1.3.2 Numerical Dispersion Control

The numerical dispersion can be reduced to any degree that is desired if one uses a fine enough FDTD mesh. This, however, increases the number of nodes and therefore also increases the computer memory and processor time required. An alternative way to decrease numerical dispersion is to improve upon the finite difference approximation of Equation (1.4). Higher-order finite difference schemes, also called multi-point schemes, are available to reduce the error in approximating the derivatives. The fourth-order-accurate schemes called FDTD(2,4) employ four nodal values located at $\Delta u/2$ and $3\Delta u/2$ on either side of the observation point u_0, and the space derivative is defined as [5]

$$\left.\frac{\partial F^n}{\partial u}\right|_{u_o} = \frac{9}{8}\left.\frac{F^n\left(u_o+\frac{\Delta u}{2}\right)-F^n\left(u_o-\frac{\Delta u}{2}\right)}{\Delta u}\right|_{\Delta u\to 0} - \frac{1}{24}\left.\frac{F^n\left(u_o+3\frac{\Delta u}{2}\right)-F^n\left(u_o-3\frac{\Delta u}{2}\right)}{\Delta u}\right|_{\Delta u\to 0} + O(\Delta u)^4 \tag{1.7}$$

Another algorithm with lower dispersion called SBTD (sampling bi-orthogonal time domain) has been proposed. It is an explicit scheme with leap-frog update. It is conditionally stable wavelet-based scheme in which spatial discretization of FDTD is replaced with sampling bi-orthogonal discretization [6]. The field is expanded in wavelets or scale functions as basis functions in space domain, while the time domain expansion is in pulse functions. The coefficients of expansion of wavelets are determined by testing Maxwell's equations with the scaling functions. For the two-dimensional TM case, the expression for the fields for SBTD is of the form [6]

$$E_z^{n+1}(i,j) = E_z^n(i,j)+\frac{\Delta t}{\varepsilon\Delta x}\sum_{p=-3}^{2} c_p H_y^{n+1/2}(i+p+\tfrac{1}{2},j)-\frac{\Delta t}{\varepsilon\Delta y}\sum_{p=-3}^{2} c_p H_x^{n+1/2}(i,j+p+\tfrac{1}{2}) \tag{1.8a}$$

$$H_y^{n+1/2}(i+\tfrac{1}{2},j) = H_y^{n-1/2}(i+\tfrac{1}{2},j)+\frac{\Delta t}{\mu\Delta x}\sum_{p=-3}^{2} c_p E_z^n(i+p+1,j) \tag{1.8b}$$

$$H_x^{n+1/2}(i,j+\tfrac{1}{2}) = H_x^{n-1/2}(i,j+\tfrac{1}{2})-\frac{\Delta t}{\mu\Delta y}\sum_{p=-3}^{2} c_p E_z^n(i,j+p+1) \tag{1.8c}$$

where

$$c_0 = 1.229167 = -c_{-1}, c_1 = -0.093750 = -c_{-2}, c_2 = 0.010417 = -c_{-3} \tag{1.9}$$

The field expressions (1.8) and (1.5) are very similar. The number of terms on the RHS of (1.8) are six compared to four for the fourth-order accurate finite difference scheme (1.7), and might be responsible for lower dispersion property of SBTD. The SBTD scheme belongs to the family of multiresolution time-domain (MRTD) schemes using Cohen-Daubechies-Feauveau (CDF) wavelets [7]. The MRTD schemes simultaneously address issues of higher-order approximation of fields, multigrid structure, and accurate treatment of the interface between different media, unlike the piecemeal approach of FDTD schemes [7].

The phase velocity for the two-dimensional TM case for SBTD and FDTD(2,2) schemes are compared in Figure 1.3 [6]. The number of nodes per wavelength or spatial resolution N is 20 and $q = 0.5$. It is observed from the graph that the phase velocity for SBTD scheme is $1.001c$ independent of the direction of travel of wave. The error is also less compared to FDTD(2,2).

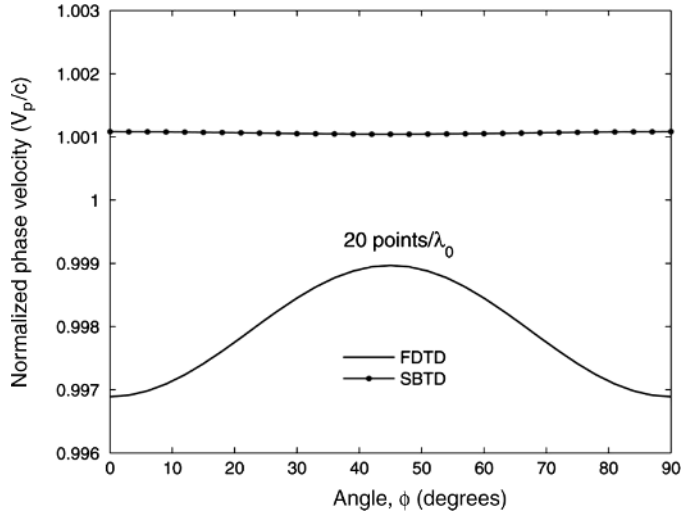

Figure 1.3 Comparison of dispersion curves for SBTD and FDTD(2,2), ($q = 0.5$). Reproduced by permission of ©2008 IEEE, Figure 1 of [6]

The normalized phase velocity for FDTD(2,2) and SBTD schemes for a cubic mesh with $N = 20$ are compared in [8] and plotted here as Figure 1.4. It is noted from Figure 1.4 that SBTD with $q = 0.5$ is isotropic and least dispersive. The combination of various spatial and temporal discretizations ($q = 0.75$) have been studied for their effect on numerical dispersion [9]. The phase velocity is plotted as a function of spatial sampling rate N in Figure 1.5 [9]. For each scheme, the phase velocity is bounded by two lines; the maximum (max) phase velocity occurs along the cell diagonal and the minimum (min) velocity occurs along the axis of the cell. It is noted from Figure 1.5 that except for FDTD(2,2), all other schemes generate fast ($>c$) waves.

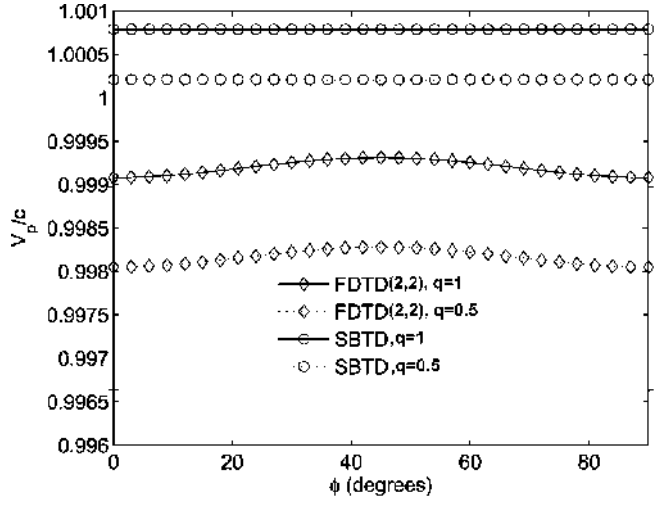

Figure 1.4 Comparison of normalized phase velocity versus azimuth angle in a cubic mesh at a spatial sampling rate of 20 points per wavelength. q is the Courant number. Reproduced by permission of ©2008 IEEE, Figure 1 of [8]

The slow and fast wave behavior of various schemes, Figure 1.5, may be exploited to reduce numerical dispersion in FDTD. For this, hybrid FDTD schemes have been proposed. The hybrid scheme based on the combination of FDTD(2,2) and FDTD(2,4) is called HFDTD(2,4), and that based on FDTD(2,2) and SBTD is called HSBTD1 [9]. Numerical dispersion produced by the hybrid schemes has been compared with non-hybrid schemes and it is found that dispersion can be minimized by properly combining the schmes with slow and fast waves [9]. The lay-out of cells for such an experiment is shown in Figure 1.6 [9]. Most of the cells are updated using higher-order schemes. The cells marked black are updated using higher-order

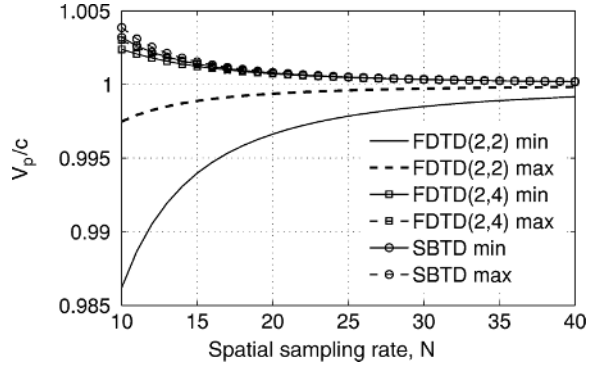

Figure 1.5 Comparison of phase velocities for SBTD and FDTD schemes as a function of spatial sampling rate N, $q = 0.75$. Reproduced by permission of ©2009 IEEE, Figure 1 of [9]

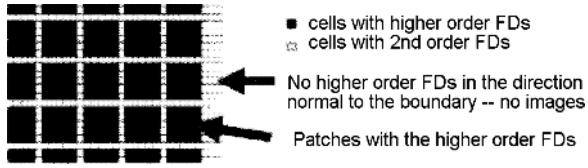

Figure 1.6 Cell pattern for the field components normal to the view. Reproduced by permission of ©2009 IEEE, Figure 2 of [9]

schemes whereas the cells marked white in each sixth row and column are updated with second-order schemes. For various schemes, the effect of spatial sampling rate or grid resolution on the error in resonant frequency of a two-dimensional cavity is compared in Figure 1.7 [9]. It is confirmed from Figure 1.7 that the hybrid schemes may be used to reduce the numerical error significantly. Further numerical experiments on a partially filled rectangular waveguide cavity confirm that the error in resonant frequency reduced by a factor of 3.1 when HFDTD(2,4) is employed; this factor increased to 22 when HSBTD1 is used. All these results are compared to standard FDTD(2,2). The spatial sampling rate used was 26.7. The processor times of the hybrid schemes are similar to those of higher-order schemes. The effects of numerical dispersion for layered, anisotropic media have been reported in [10].

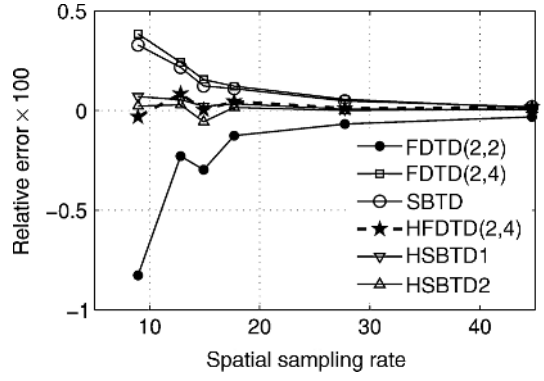

Figure 1.7 Comparison of relative error of various schemes for the resonant frequency of a two-dimensional rectangular cavity. Reproduced by permission of ©2009 IEEE, Figure 3 of [9]

One area of challenge in applying the higher-order and hybrid schemes is in the treatment of boundary conditions which are inside the computational domain, e.g. antenna conductors, feed lines, pins, dielectric interface, etc. [5]. Some of these issues for standard FDTD method are discussed in [11]. Lossy curved surface in the form of surface impedance boundary condition is modeled in [12]. The metal-semiconductor interfaces may be defined by higher-order impedance boundary conditions [13].

Numerical dispersion exhibited by the various finite difference schemes have been reviewed and expressed in the form of a general expression [8]:

$$\cos(\omega\Delta t) = \mathrm{Re}(\lambda_k) \tag{1.10}$$

where λ_k is the complex eigenvalue (not equal to unity) of the amplification matrix M. The above expression is applicable to all known conditionally and unconditionally stable algorithms; within their stability limits for conditionally stable schemes. For specific FDTD schemes, expression for λ_k in terms of discretization parameters and numerical wave number is available in [8]. For FDTD(2,2), the eigenvalues of M are obtained as $\lambda_{1,2} = 1$, $\lambda_{3,4,5,6} = 1-2d \pm 2j\sqrt{d(1-d)}$, where d is given by [8]

$$d = q_x^2 \sin^2(\phi_x/2)+q_y^2 \sin^2\big(\phi_y/2\big)+q_z^2 \sin^2(\phi_z/2) \tag{1.11a}$$

$$q_u = c\Delta t/\Delta u \quad R_u = \lambda/\Delta u \quad k_0 = 2\pi/\lambda \;\; u : x, y \quad \text{or } z \tag{1.11b}$$

$$\phi_x = \frac{2\pi}{R_x}\frac{k_{num}}{k_0}\sin\theta\, cos\,\phi \quad \phi_y = \frac{2\pi}{R_y}\frac{k_{num}}{k_0}\sin\theta\sin\phi \quad \phi_z = \frac{2\pi}{R_z}\frac{k_{num}}{k_0}\cos\theta \tag{1.11c}$$

1.4 Stability of Algorithms

The stability requirement of algorithm (1.5) puts an *upper limit* on time step Δt. This limit is necessary otherwise the computed field values might increase spuriously without limit as time marching continues. The reason for numerical instability is the violation of causality, that is, the minimum time Δt required for the signal to propagate from one node to the other separated by Δ is given by $\Delta t = \Delta/c$. Increasing the value of Δt beyond this value to speed up the simulation will result in instability. The upper bound on Δt is called the CFL *stability condition* or sometimes Courant limit and is given by (1.1). For the special case of cubic cell $\Delta x = \Delta y = \Delta z = \Delta$, one obtains

$$c.\Delta t_{CFL} \leq \frac{\Delta}{\sqrt{3}} \tag{1.12}$$

The stability and numerical dispersion for ADI, CNSS and CN schemes are investigated in terms of their amplification matrix M [14]. The ADI and CNSS schemes are found to have the same dispersion,. and CN and CNSS are found to be unconditionally stable. However, the unconditional stablility of ADI is contingent upon space-time discretizations, and its amplification matrix M is given by

$$||M_{ADI}|| \leq \sqrt{1+\left(\frac{c\Delta t}{min(\Delta x, \Delta y, \Delta z)}\right)^2} \tag{1.13}$$

where the matrix M is a function of wavenumber(magnitude and propagation direction), and space-time discretizations $\Delta x, \Delta y, \Delta z, \Delta t$. For a cubic cell, (1.13) reduces to

$$||M_{ADI}|| \leq \sqrt{1+\frac{q^2}{3}} \tag{1.14}$$

Another unconditionally stable FDTD scheme is LOD-FDTD. It is an efficient scheme compared to ADI, CN and CNSS schemes and is described in Section 1.5.

The FDTD algorithm may have to be run for a large number of time steps, sometimes of the order of 100,000 steps until the time domain waveform converges. It is possible to accelerate the convergence of the algorithm by using matrix-pencil (or GPOF) approach [15]. In this approach, the late time waveform can be predicted from the early time sampling data. One may be able to save about 80% of the simulation time using GPOF [16].

1.5 Absorbing Boundary Conditions

The antennas have associated open space region. The FDTD simulation of the antenna in this form will require an unlimited amount of computer memory and processing time, which is impossible to arrange. Therefore, the domain must be truncated so that the associated reflection is minimal. For this, the solution domain is divided into two regions: the interior region and the exterior region as shown in Figure 1.8. The interior region must be large enough to enclose the antenna of interest. The exterior region simulates the infinite space. It is a limited free space enclosing the interior region on one side and terminated on the other side by a perfect electric conductor. When we apply the FDTD algorithm to the interior region, it simulates wave propagation in the forward and backward directions. However, only the outward propagation in the exterior region is desired so that infinite free space conditions are simulated. Reflections are generated at the interior-exterior region interface and from the perfect electric conductor terminating the exterior region. These reflections must be suppressed to an acceptable level so that the FDTD solution is valid for all time steps. The exterior region includes the domain of absorbing boundary condition or ABC for short.

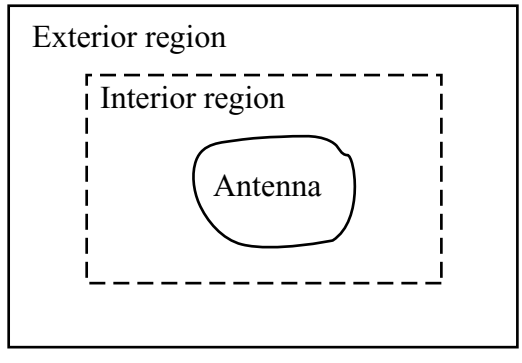

Figure 1.8 A typical truncation of the physical domain by the exterior region in FDTD algorithms

The absorbing boundary condition can be simulated in a number of ways. These are classified as analytical (or differential) ABC and material ABC. The material ABC is realized from the physical absorption of the incident wave by means of a lossy medium, whereas analytical ABC is simulated by approximating the one-way wave equation on the boundary of interior region. Whereas the analytical ABC may be able to provide upto -60 dB of reflection, the material ABC can provide better absorption with the reflection reaching an

ideal limit of −80 to −120 dB from PML at the boundaries. Various types of ABCs are summarized next.

1.5.1 Analytical Absorbing Boundary Conditions

Analytical ABC is a popular technique because of its simplicity of implementation. The reflection from analytical ABC could be as low as 0.1%, i.e. −60 dB. Analysis for this absorbing boundary condition is based on the works of Enquist and Majda [17], Mur [18], Higdon [19], and Liao [20]. For a plane wave incident on a planar boundary, the wave will propagate forward (without any reflection) if the field function $F(x,y,z,t)$ satisfies one-way wave equation at the boundary. Such a boundary is therefore called the absorbing boundary. The PDE for the ABCs may be derived from the wave equation. Consider the following two-dimensional wave equation in the Cartesian coordinates

$$\frac{\partial^2 F}{\partial x^2}+\frac{\partial^2 F}{\partial y^2}-\frac{1}{c^2}\frac{\partial^2 F}{\partial t^2}=0 \tag{1.15}$$

This expression may be factored as

$$\left(\frac{\partial}{\partial x}-\sqrt{\frac{1}{c^2}\frac{\partial^2}{\partial t^2}-\frac{\partial^2}{\partial y^2}}\right)\left(\frac{\partial}{\partial x}+\sqrt{\frac{1}{c^2}\frac{\partial^2}{\partial t^2}-\frac{\partial^2}{\partial y^2}}\right)F=0 \tag{1.16}$$

Applying each of the above pseudo-operators to F gives rise to the following PDEs for the analytical ABC as

$$\left(D_x-\frac{D_t}{c}\sqrt{1-s^2}\right)F=0 \quad \text{for ABC on the left boundary} \tag{1.17a}$$

$$\left(D_x+\frac{D_t}{c}\sqrt{1-s^2}\right)F=0 \quad \text{for ABC on the right boundary} \tag{1.17b}$$

where $D_x=\partial/\partial x$, etc. and $s=cD_y/D_t$. Direct implementation of the operators with square root is not possible. The operators are therefore approximated and result in various forms of ABC depending on the approximation employed.

The first-order ABCs are obtained by a very crude approximation $\sqrt{1-s^2}\approx 1$ in (1.17a); one obtains

$$\left(\frac{\partial}{\partial x}-\frac{1}{c}\frac{\partial}{\partial t}\right)F|_{x=0}=0 \tag{1.18}$$

for the left boundary at $x=0$. Similar expressions can be written down by inspection for the other boundaries also. The expression (1.18) is called the Enquist-Majda (E-M) first-order ABC. The field function F represents the electric field tangential to the boundary. For a non-planar wave, Equation (1.18) should be applied to all the components tangential to the planar boundary. It is shown that (1.18) is unconditionally stable [18]. The absorbing boundary condition (1.18) is exact only for a plane wave at normal incidence. Hence the wave will be

reflected for an oblique incidence. Higher-order ABCs are suitable for non-normal incidence, and are obtained by better approximation of the square root function $\sqrt{1-s^2}$. For this, let us approximate $\sqrt{1-s^2}$ in a general form as

$$\sqrt{1-s^2} \approx \frac{d-bs^2}{1-as^2} \tag{1.19}$$

where the parameters a, b, d are optimized to define various forms of third-order ABCs such as Chebyshev, Pade and EM second-order. Use of Equation (1.19) in Equation (1.17a) gives

$$\frac{\partial^3 F}{\partial x \partial t^2} - ac^2 \frac{\partial^3 F}{\partial x \partial y^2} - \frac{d}{c}\frac{\partial^3 F}{\partial t^3} + bc \frac{\partial^3 F}{\partial t \partial y^2} = 0 \tag{1.20}$$

This expression reduces to:

(a) first-order E-M ABC for $d=1$, $a=b=0$;
(b) second-order E-M ABC for $d=1$, $b={}^1/_2$, $a=0$;
(c) Pade approximation or Pade ABC for $d=1$, $b={}^3/_4$, $a={}^1/_4$;
(d) Chebyshev ABC for $d=0.99973$, $b=0.80864$, $a=0.31657$.

Mur's ABCs are discretized versions of E-M ABCs, e.g. first-order Mur ABC for the boundary at $x=0$ is obtained by discretizing Equations (1.17a) or (1.20) at $x=\Delta x/2$, $t=(n+1/2)\Delta t$ and is given by

$$F_0^{n+1} = F_{\mathbf{1}}^{\mathbf{n}} + \left(\frac{c\Delta t - \Delta x}{c\Delta t + \Delta x}\right)\left(F_1^{n+1} - F_0^n\right) \tag{1.21}$$

Similar expressions may be obtained for other types of ABCs and for waves incident on different boundaries. One can realize about -40 dB reflection by using these ABCs. Liao's third-order ABC may be used to achieve about -50 to -60 dB reflection and is discussed next.

1.5.1.1 Liao's ABC

Liao's ABC is based on the extrapolation of fields in time and space using Newton-backward difference polynomial. Consider an outer grid boundary at $i_{\max} = M\Delta x$, then the L-th order Liao ABC may be written as [2, 21]

$$F^{n+1}(i_{\max}) = \sum_{l=1}^{L} (-1)^{l+1} C_l^L F^{n+1-l}(i_{\max} - lh) \tag{1.22}$$

where $h = \alpha c\Delta t/\Delta x$, α is the damping factor $0 \le \alpha \le 2$, and C_l^L is the Binomial coefficient defined as

$$C_l^L = \frac{L!}{l!(L-l)!} \tag{1.23}$$

It may be noted from Equation (1.22) that the field values at different time instants $(n+1-l)\Delta t$ and different locations $(i_{\max}-lh)\Delta x$ are combined judiciously to produce a near null field $F^{n+1}(i_{\max})$. This scheme is different from the one-way wave equation scheme and is found to be stable with double precision computations [2]. The choice of α and therefore h is not critical in Equation (1.22), resulting in the robustness of the scheme. The value of α may be chosen such that h is an integer and the required field locations coincide with those available in the standard FDTD scheme. Otherwise, quadratic interpolation may be employed. For the third-order ABC and h an integer, Equation (1.22) becomes

$$F_M^{n+1} = 3F_{M-1}^{n} - 3F_{M-2}^{n-1} + F_{M-3}^{n-2} \tag{1.24}$$

where F is one of the electric field components tangential to the boundary.

Interpretation of analytical ABCs in terms of surface impedance boundary condition (SIBC) is discussed in [22]. The SIBC involves tangential components of both E and H fields, whereas other analytical ABCs are applied to E field only. The SIBC type ABCs reduce the order of PDE without compromising the performance and this is discussed next.

Consider the half-space of an isotropic medium terminating the problem physical domain as shown in Figure 1.9. The interface is defined by $z = 0$. Equating the tangential components of E and H at the interface gives [23]

$$k_0\sqrt{k_0^2 - k_x^2 - k_y^2}\, E_x = -\eta_0\left[\left(k_0^2 - k_x^2\right)H_y + k_x\, k_y\, H_x\right] \tag{1.25a}$$

$$k_0\sqrt{k_0^2 - k_x^2 - k_y^2}\, E_y = \eta_0\left[\left(k_0^2 - k_y^2\right)H_x + k_x\, k_y\, H_y\right] \tag{1.25b}$$

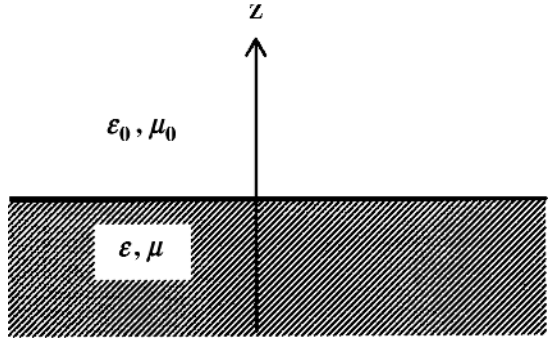

Figure 1.9 Half-space termination of physical space for deriving surface impedance boundary condition

For the two-dimensional TM_x waves ($H_x = 0$) with the fields constant along x ($k_x = 0$), Equation (1.25) reduces to

$$\sqrt{k_0^2 - k_y^2}\, E_x = -\eta_0 k_0 H_y \tag{1.26}$$

Approximating the square-root factor according to Equation (1.19) gives

$$\left(dk_0^2 - bk_y^2\right)E_x = -\eta_0\left(k_0^2 - ak_y^2\right)H_y \tag{1.27}$$

The corresponding partial differential equation (PDE) for this boundary condition is obtained by using $k_0^2 = \omega^2/c^2$, $j\omega \leftrightarrow \partial/\partial t$, and $-jk_y = \partial/\partial y$ [23]

$$\frac{d}{c^2}\frac{\partial^2 E_x}{\partial t^2} - b\frac{\partial^2 E_x}{\partial y^2} = -\frac{\eta_0}{c^2}\frac{\partial^2 H_y}{\partial t^2} + \eta_0 a\frac{\partial^2 H_y}{\partial y^2} \tag{1.28}$$

It may be recast in the following form by using $\dfrac{\partial^2 H_y}{\partial t^2} = -\dfrac{c}{\eta_0}\dfrac{\partial^2 E_x}{\partial z \partial t}$

$$\frac{d}{c^2}\frac{\partial^2 E_x}{\partial t^2} - b\frac{\partial^2 E_x}{\partial y^2} = \frac{1}{c}\frac{\partial^2 E_x}{\partial z \partial t} + \eta_0 a\frac{\partial^2 H_y}{\partial y^2} \tag{1.29}$$

Discretizing it about the point $x = i\Delta x, y = \Delta y/2$ at $t = n\Delta t$ gives [23]

$$\begin{aligned} E_x|_{i,0}^{n+1} = {} & -E_x|_{i,0}^{n-1} + \frac{2d\Delta z}{c\Delta t + d\Delta z}\left(E_x|_{i,0}^{n} + E_x|_{i,1}^{n}\right) + \frac{c\Delta t - d\Delta z}{c\Delta t + d\Delta z}\left(E_x|_{i,1}^{n+1} + E_x|_{i,0}^{n-1}\right) \\ & + \frac{b(c\Delta t)^2\Delta z}{\Delta y^2(c\Delta t + d\Delta z)}\begin{pmatrix} E_x|_{i+1,1}^{n} - 2E_x|_{i,1}^{n} + E_x|_{i-1,1}^{n} \\ + E_x|_{i+1,0}^{n} - 2E_x|_{i,0}^{n} + E_x|_{i-1,0}^{n} \end{pmatrix} \\ & + \frac{\eta_0 a(c\Delta t)^2\Delta z}{\Delta y^2(c\Delta t + d\Delta z)}\begin{pmatrix} H_y|_{i+1,1/2}^{n+1/2} - 2H_y|_{i,1/2}^{n+1/2} + H_y|_{i-1,1/2}^{n+1/2} \\ + H_y|_{i+1,1/2}^{n-1/2} - 2H_y|_{i,1/2}^{n-1/2} + H_y|_{i-1,1/2}^{n-1/2} \end{pmatrix} \end{aligned} \tag{1.30}$$

The above expression reduces to first-order Mur ABC for $d = 1$, $a = b = 0$; second-order Mur ABC for $d = 1$, $b = {}^1/_2$, $a = 0$; Pade ABC for $d = 1$, $b = {}^3/_4$, $a = {}^1/_4$; and Chebyshev ABC for $d = 0.99973$, $b = 0.80864$, $a = 0.31657$.

The numerical results based on Equation (1.30) show that the second-order PDE (1.29) involving both the components of E and H have similar performance as the third-order PDE of (1.20) for one field component [22].

The performance of an ABC is determined by the power reflected by it and summed over the whole grid. It is called global error and is defined as

$$E = \sum\sum\sum e^2(i,j,k) \tag{1.31}$$

where e is the amplitude of reflected wave for an incident wave of unit amplitude. The expression (1.30) was implemented for SIBC-based Chebyshev and Pade ABC, and compared with Liao's third-order and Mur's second-order ABC on 20×200 lattice. The source was a Gaussian-like pulse of width $30\Delta t$. The global error as a function of time is compared in Figure 1.10 [22]. It may be noted that the second-order SIBC (Pade and Chebyshev) performs

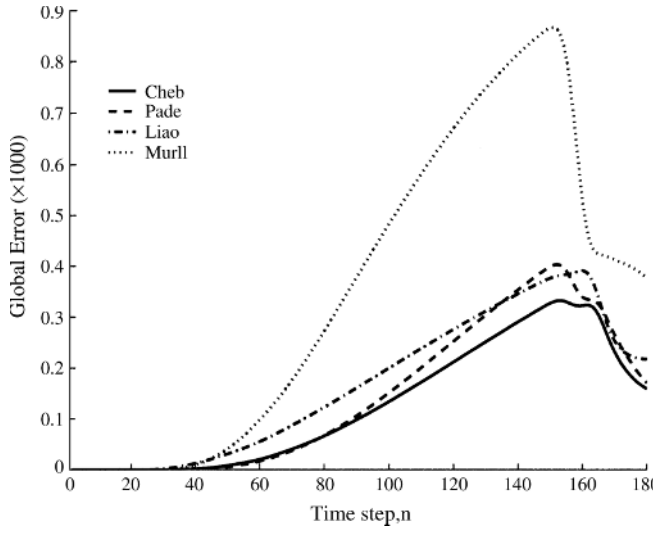

Figure 1.10 Comparison of global error as a function of time for SIBC-based Chebyshev and Pade ABCs with Liao's and Mur's second-order ABCs. Reproduced by permission of ©2003 IEEE, Figure 2 of [22]

much better than the second-order Mur's ABC. The Chebyshev approximation is better than the third-order Liao ABC. The decay in global error after about $n = 150$ is due to the fact that the source pulse went to zero some time ago. Extension of SIBC-based ABC for the three-dimensional case is also discussed in [22].

Perfectly matched layer (PML) may be employed for lower reflections and is discussed next. The performance of some of the higher-order analytical ABCs is compared with PML in [24]. The golobal error for $30 \times 30 \times 30$ geometry is compared in Figure 1.11 for higher-order analytical ABCs and PML [24]. The Gaussian-like excitation pulse is $40\,\Delta t$ wide. The PML was terminated with Liao's ABC instead of electric wall. The difference between third-order E-M and Liao's fifth-order is about 20 dB. It may be observed that PML can provide an excellent termination of space domain.

1.5.2 Material-Absorbing Boundary Conditions

The absorbing sheets method was the first material ABC proposed and was used for FDTD computations by Hallond and Williams [25]. In this method the exterior region is filled with a lossy medium with parameters $(\mu', \varepsilon', \sigma^*, \sigma)$, where σ is the electrical conductivity and σ^* is the fictitious magnetic conductivity. The lossy medium is taken to be of finite thickness and is backed by a perfect electric conductor. The values of σ and σ^* are selected so that when a wave is incident normal to the interface separating the free space interior region and the lossy medium, there should be no reflection, which is possible only if

$$Z_0 = Z_m \tag{1.32}$$

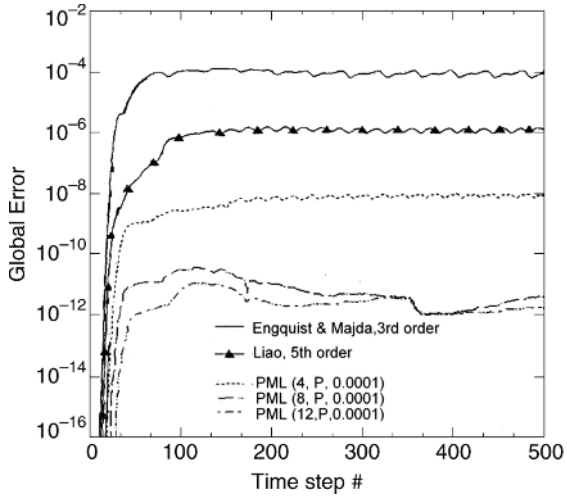

Figure 1.11 Comparison of global error as a function of time for a number of higher-order ABCs and PML. Reproduced by permission of ©1997 IEEE, Figure 1 of [24]

where Z_0 is the free space impedance defined by $(\mu_o, \varepsilon_o, \sigma^* = 0, \sigma = 0)$ and Z_m is the impedance of the lossy medium dependent on $(\mu', \varepsilon', \sigma^*, \sigma)$. Equation (1.32) can be expressed as

$$\sqrt{\frac{\mu_0}{\varepsilon_0}} = \sqrt{\frac{\mu' + j\sigma^*}{\varepsilon' + j\sigma}} \tag{1.33}$$

For convenience if we choose $\mu' = \mu_0$, $\varepsilon' = \varepsilon_0$ then matching condition (1.33) yields

$$\frac{\sigma^*}{\mu_0} = \frac{\sigma}{\varepsilon_0} = v \tag{1.34}$$

In practice, the conductivity of the lossy medium is increased gradually from 0 to σ_m at the thickness t of the lossy medium. The increase may be linear or parabolic, and σ is written as $\sigma(\rho)$ where ρ is the distance from the interface.

The magnitude of the reflection coefficient for a wave incident at an angle ϕ w.r.t the normal to the layers is

$$R(\phi) = [R(0)]^{\cos(\phi)} \tag{1.35}$$

with R(0) the reflection coeffficient for normal incidence and is defined as

$$R(0) = \exp\left(\frac{-2}{\varepsilon_o c}\int_0^t \sigma_n(\rho)d\rho\right) \qquad n = 0, 1, 2\ldots \tag{1.36}$$

In general, the profile for the PML medium may be defined as

$$\sigma_n(\rho) = \sigma_m\left(\frac{\rho}{t}\right)^n \tag{1.37}$$

and the corresponding

$$R(0) = \exp\left(\frac{-2\sigma_m t}{(n+1)\varepsilon_o c}\right) \quad n = 0, 1, 2\ldots \tag{1.38}$$

It appears from (1.38) that one may choose a sufficiently thick lossy medium to obtain any desired amount of reflection. However, the reflection at oblique incident angles is higher, and the total reflection at the interface for the absorbing sheets method is of the same order as that obtained from analytical ABCs discussed earlier.

1.5.3 Perfectly Matched Layer ABC

The perfectly matched layer (PML) formulation was proposed by Berenger [26] and represents a generalization of the absorbing sheets method to arbitrary angles of incidence. This is achieved by splitting the electric and magnetic field components in the absorbing media, and assigning different losses along different axis. The net effect of this is to create a nonphysical lossy medium in the exterior region so that the wave impedance in this medium is independent of the angle of incidence and frequency of the waves. The split-field PML makes coding difficult. However, this method is used as a benchmark for other PML formulations.

1.5.4 Uniaxial PML

Non-split field formulations in PML have been developed to simplify coding. One of these formulations is in the form of complex stretching of the Cartesian coordinates in the frequency domain [27]. The stretching variable formulation leads to convolution in the time domain, and can be avoided by the splitting of fields similar to that in Berenger's PML.

In a popular unsplit-field formulation, the PML medium employed is anisotropic with permittivity and permeability tensors, and is called Uniaxial PML, UPML for short. The general formulation for UPML is given in [28, 29]. A diagonal tensor is uniaxial if it is anisotropic along one axis only and is defined as

$$\bar{\bar{\varepsilon}} = \varepsilon_0\bar{\bar{s}}, \quad \text{and} \quad \bar{\bar{\mu}} = \mu_0\bar{\bar{s}} \tag{1.39}$$

where the media tensor $\bar{\bar{s}}$ for the three-dimensional PML region is defined as [30]

$$\bar{\bar{s}} = \begin{bmatrix} 1/s_x & 0 & 0 \\ 0 & s_x & 0 \\ 0 & 0 & s_x \end{bmatrix} \begin{bmatrix} s_y & 0 & 0 \\ 0 & 1/s_y & 0 \\ 0 & 0 & s_y \end{bmatrix} \begin{bmatrix} s_z & 0 & 0 \\ 0 & s_z & 0 \\ 0 & 0 & 1/s_z \end{bmatrix} = \begin{bmatrix} s_y s_z/s_x & 0 & 0 \\ 0 & s_z s_x/s_y & 0 \\ 0 & 0 & s_x s_y/s_z \end{bmatrix} \tag{1.40}$$

and s_v are defined as

$$s_v = k_v + \frac{\sigma_v}{j\omega\varepsilon} = k_v + \frac{\rho_v}{j\omega\mu} \qquad v = x, y, z \tag{1.41}$$

where σ_v and ρ_v are the UPML medium conductivity and reluctivity along the v-axis, respectively. The medium characterized as above leads to reflectionless propagation from free space to PML for both TE and TM waves, independent of angle of incidence, polarization and frequency. For exponential decay of the propagating wave in UPML, the media constants should be complex with $s_v = 1 + \frac{\sigma_v}{j\omega\varepsilon}$. The UPML is characterized by $\sigma_x(i)$ alone for layers perpendicular to x-axis, by $\sigma_y(j)$ alone for layers perpendicular to y-axis, by $\sigma_x(i)$and $\sigma_y(j)$ etc. for the edge regions, and by $\sigma_x(i)$, $\sigma_y(j)$ and $\sigma_z(k)$ for the corner regions as shown in Figure 1.12. The non-PML region or central region is characterized by $\sigma_x = \sigma_y = \sigma_z = 0$, thus simplifying coding. The values of σ_v are gradually increased as one goes deeper into the PML region.

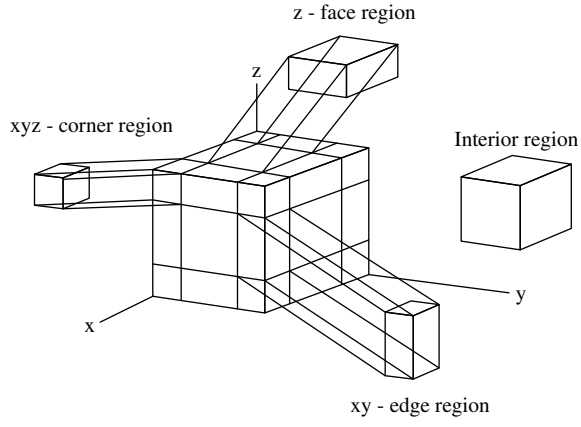

Figure 1.12 Illustration showing the face, edge and corner regions of the PML medium surrounding the interior region

The implementation of UPML in FDTD algorithm is not simple since the medium is dispersive due to the frequency dependence of permittivity and permeability tensors. Direct transformation from frequency domain to time domain involves convolution and is inefficient. Instead, a two-step time marching scheme is suggested in [2] for efficient implementation of UPML. In this scheme Maxwell's equations are formulated in terms of D and B, and E and H are derived from these. The procedure reported in [30] is D(E)-H based which can be easily implemented in most of the FDTD schemes, e.g. for the standard FDTD scheme

$$
\begin{aligned}
D_x^{n+1}(i+\tfrac{1}{2},j,k) \quad &= c_j^1 D_x^n(i+\tfrac{1}{2},j,k) \\
&+c_j^2\left(\frac{H_z^{n+1/2}(i+\frac{1}{2},j+\frac{1}{2},k)-H_z^{n+1/2}(i+\frac{1}{2},j-\frac{1}{2},k)}{\Delta y}\right. \\
&\left.-\frac{H_y^{n+1/2}(i+\frac{1}{2},j,k+\frac{1}{2})-H_y^{n+1/2}(i+\frac{1}{2},j,k-\frac{1}{2})}{\Delta z}\right)
\end{aligned} \tag{1.42}
$$

where

$$
c_j^1 = \frac{2\varepsilon k_y-\sigma_y(j)\Delta t}{2\varepsilon k_y+\sigma_y(j)\Delta t},\ c_j^2 = \frac{2\varepsilon\Delta t}{2\varepsilon k_y+\sigma_y(j)\Delta t} \tag{1.43}
$$

$$
E_x^{n+1}(i+\tfrac{1}{2},j,k) = c_k^3\,E_x^n(i+\tfrac{1}{2},j,k)+c_k^4\left(c_{i+1/2}^5\,D_x^{n+1}(i+\tfrac{1}{2},j,k)-c_{i+1/2}^6\,D_x^n(i+\tfrac{1}{2},j,k)\right) \tag{1.44}
$$

where

$$
\begin{aligned}
&c_k^3 = \frac{2\varepsilon k_z-\sigma_z(k)\Delta t}{2\varepsilon k_z+\sigma_z(k)\Delta t}, \quad c_k^4 = \frac{1}{\varepsilon(2\varepsilon k_z+\sigma_z(k)\Delta t)}, \\
&c_{i+1/2}^5 = 2\varepsilon k_x+\sigma_x(i+1/2)\Delta t, \quad c_{i+1/2}^6 = 2\varepsilon k_x-\sigma_x(i+1/2)\Delta t
\end{aligned} \tag{1.45}
$$

It is understood that the indices i,j,k within the brackets after σ_x, etc. refer to the position of the node.

Substituting for D_x^{n+1} from Equation (1.42), one can write,

$$
\begin{aligned}
E_x^{n+1}(i+\tfrac{1}{2},j,k) \quad &= c_k^3 E_x^n(i+\tfrac{1}{2},j,k)+\left(c_k^4 c_{i+1/2}^5 c_j^1-c_k^4 c_{i+1/2}^6\right)D_x^n(i+\tfrac{1}{2},j,k) \\
&+c_k^4 c_{i+1/2}^5 c_j^2\left(\frac{H_z^{n+1/2}(i+\frac{1}{2},j+\frac{1}{2},k)-H_z^{n+1/2}(i+\frac{1}{2},j-\frac{1}{2},k)}{\Delta y}-\right. \\
&\left.\frac{H_y^{n+1/2}(i+\frac{1}{2},j,k+\frac{1}{2})-H_y^{n+1/2}(i+\frac{1}{2},j,k-\frac{1}{2})}{\Delta z}\right)
\end{aligned} \tag{1.46}
$$

Similar expressions may be obtained for other field components. For a two-dimensional PML, the updating equations are obtained by setting $\sigma_z = 0, k_z = 1$. The optimal value of σ_v used in the updating equations may be chosen according to that given in [31, 32].

The numerical results for FDTD(2,2), SBTD, ADI, and CN schemes employing this UPML are presented for two-dimensional TE cases in [30]. The absorbing behavior of UPML for SBTD scheme is found to be similar to that for FDTD(2,2). The UPML in ADI scheme is found to produce larger reflections compared to that in FDTD(2,2) and is shown in Figure 1.13 for the three-dimensional study [32]. The value of Δt_{CFL} used is 1.926 ps. Also, the absorbing ability of UPML deteriorates with the increase in Courant number q in Figure 1.13. The reflection error is defined as $\left|E_{measured} - E_{ref}\right| / \left|E_{ref\ \max}\right|$ where E_{ref} is the value measured by extending the dimensions outward to avoid reflections from boundaries, and $E_{ref\ \max}$ is the maximum value observed at the same point.

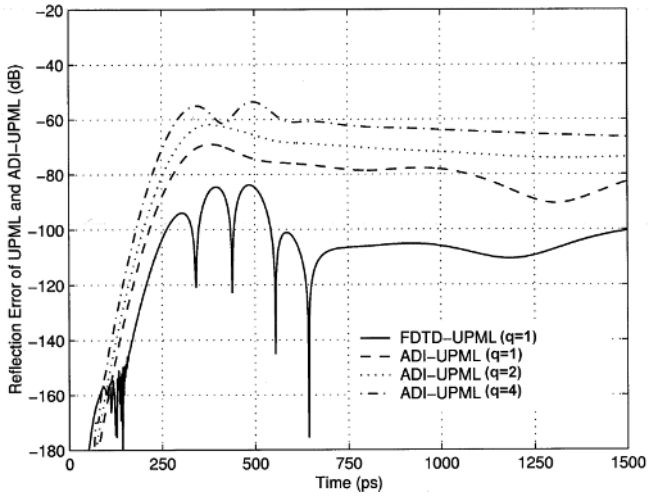

Figure 1.13 Reflection error from the FDTD-UPML and ADI-UPML as a function of time with q as a parameter. Reproduced by permission of ©2002 IEEE, Figure 1 of [32]

1.6 LOD-FDTD Algorithm

The alternating-direction implicit (ADI) FDTD algorithm was proposed by Namiki [33]. It employs the same grid as in FDTD(2,2) and is second-order accurate in both space and time. The algorithm is implicit because the update of fields is not a single step process as for FDTD(2,2) but involves solving a set of simultaneous equations as an intermediate step. The ADI algorithm has been analyzed thoroughly for its dispersion and stability properties. It has been found that the maximum permissible step size Δt in ADI-FDTD depends on the numerical errors which increase with the increase in the Courant number q. ADI exhibits splitting error which depends not only on time step size but also on the spatial derivatives of fields. Due to its implicit nature which involves solving a tridiagonal matrix equation, the number of arithmetic operations per update of fields is more compared to FDTD(2,2). CN-FDTD is more accurate than ADI-FDTD but is computationally expensive. The LOD-FDTD is simple to code, is 20% more efficient, and provides similar accuracy as ADI-FDTD for the same computer memory

required [34]. We describe LOD-FDTD algorithm for three-dimensional problems next. The efficiency of LOD-FDTD can be improved to 83% by a simple transformation.

For a lossless medium the Maxwell's curl equations (1.3) reduce to

$$\nabla \times \mathbf{H} = \varepsilon \frac{\partial \mathbf{E}}{\partial \mathbf{t}} \qquad \nabla \times \mathbf{E} = -\mu \frac{\partial \mathbf{H}}{\partial \mathbf{t}} \tag{1.47}$$

These equations may be expressed in operator form as

$$\frac{\partial \mathbf{F}}{\partial t} = [A]\mathbf{F} + [B]\mathbf{F} \tag{1.48}$$

where $\mathbf{F} = [E_x, E_y, E_z, H_x, H_y, H_z]^T$ and

$$[A] = \begin{bmatrix} 0 & 0 & 0 & 0 & 0 & \frac{\partial}{\varepsilon \partial y} \\ 0 & 0 & 0 & \frac{\partial}{\varepsilon \partial z} & 0 & 0 \\ 0 & 0 & 0 & 0 & \frac{\partial}{\varepsilon \partial x} & 0 \\ 0 & \frac{\partial}{\mu \partial z} & 0 & 0 & 0 & 0 \\ 0 & 0 & \frac{\partial}{\mu \partial x} & 0 & 0 & 0 \\ \frac{\partial}{\mu \partial y} & 0 & 0 & 0 & 0 & 0 \end{bmatrix} \tag{1.49a}$$

$$[B] = \begin{bmatrix} 0 & 0 & 0 & 0 & -\frac{\partial}{\varepsilon \partial z} & 0 \\ 0 & 0 & 0 & 0 & 0 & -\frac{\partial}{\varepsilon \partial x} \\ 0 & 0 & 0 & -\frac{\partial}{\varepsilon \partial y} & 0 & 0 \\ 0 & 0 & -\frac{\partial}{\mu \partial y} & 0 & 0 & 0 \\ -\frac{\partial}{\mu \partial z} & 0 & 0 & 0 & 0 & 0 \\ 0 & -\frac{\partial}{\mu \partial x} & 0 & 0 & 0 & 0 \end{bmatrix} \tag{1.49b}$$

By applying the CN (Crank-Nicolson) algorithm

$$\partial F^{(n+1/2)}/\partial t \approx (F^{n+1}-F^n)/\Delta t, \quad F^{n+1/2} \approx (F^{n+1}+F^n)/2 \tag{1.50}$$

to Equation (1.48) at $t = (n+1/2)\Delta t$ we have

$$\left([I]-\frac{\Delta t}{2}[A]-\frac{\Delta t}{2}[B]\right)\mathbf{F}^{n+1} = \left([I]+\frac{\Delta t}{2}[A]+\frac{\Delta t}{2}[B]\right)\mathbf{F}^{n} \tag{1.51}$$

Equation (1.51) can be approximated as, assuming $(\Delta t)^2 AB \ll 4$,

$$\left([I]-\frac{\Delta t}{2}[A]\right)\left([I]-\frac{\Delta t}{2}[B]\right)\mathbf{F}^{n+1} = \left([I]+\frac{\Delta t}{2}[A]\right)\left([I]+\frac{\Delta t}{2}[B]\right)\mathbf{F}^{n} \tag{1.52}$$

The above expresssion may be decomposed into the following sub-steps *if the operator matrices A and B commute*,

$$\left([I]-\frac{\Delta t}{2}[A]\right)\mathbf{F}^{n+1/2} = \left([I]+\frac{\Delta t}{2}[A]\right)\mathbf{F}^{n} \tag{1.53a}$$

$$\left([I]-\frac{\Delta t}{2}[B]\right)\mathbf{F}^{n+1} = \left([I]+\frac{\Delta t}{2}[B]\right)\mathbf{F}^{n+1/2} \tag{1.53b}$$

The splitting of time step as defined above is found to suffer from non-commutivity-related error. A simple modification of the time instant for the sub-steps is proposed to reduce this error [35]. The modification is to re-define (1.53) as

$$\left([I]-\frac{\Delta t}{2}[A]\right)\mathbf{F}^{n+3/4} = \left([I]+\frac{\Delta t}{2}[A]\right)\mathbf{F}^{n+1/4} \tag{1.54a}$$

$$\left([I]-\frac{\Delta t}{2}[B]\right)\mathbf{F}^{n+5/4} = \left([I]+\frac{\Delta t}{2}[B]\right)\mathbf{F}^{n+3/4} \tag{1.54b}$$

The change-over from the fractional time steps to integer time steps for compatibility with FDTD(2,2) will be discussed at the end. Now we substitute the operator matrices and obtain the following expressions for the field components:
Sub-step 1

$$E_x^{n+3/4} = E_x^{n+1/4}+\frac{\Delta t}{2\varepsilon}\left(\frac{\partial H_z^{n+3/4}}{\partial y}+\frac{\partial H_z^{n+1/4}}{\partial y}\right), \tag{1.55a}$$

$$H_z^{n+3/4} = H_z^{n+1/4}+\frac{\Delta t}{2\mu}\left(\frac{\partial E_x^{n+3/4}}{\partial y}+\frac{\partial E_x^{n+1/4}}{\partial y}\right) \tag{1.55b}$$

Sub-step 2

$$E_x^{n+5/4} = E_x^{n+3/4} + \frac{\Delta t}{2\varepsilon}\left(\frac{\partial H_z^{n+5/4}}{\partial y} + \frac{\partial H_z^{n+3/4}}{\partial y}\right), \tag{1.56a}$$

$$H_z^{n+5/4} = H_z^{n+3/4} + \frac{\Delta t}{2\mu}\left(\frac{\partial E_x^{n+5/4}}{\partial y} + \frac{\partial E_x^{n+3/4}}{\partial y}\right) \tag{1.56b}$$

The expressions for other field components can be simply written down by inspection.

Eliminating $H_z^{n+3/4}$ from (1.55a) and (1.55b) gives

$$E_x^{n+3/4} - \frac{\Delta t^2}{4\mu\varepsilon}\frac{\partial^2 E_x^{n+3/4}}{\partial y^2} = E_x^{n+1/4} + \frac{\Delta t^2}{4\mu\varepsilon}\frac{\partial^2 E_x^{n+1/4}}{\partial y^2} + \frac{\Delta t}{\varepsilon}\frac{\partial H_z^{n+1/4}}{\partial y} \tag{1.57}$$

The finite difference approximation of the above leads to the following update [35]

$$\begin{aligned} &-aE_x^{n+3/4}(i+\tfrac{1}{2},j-1,k)+(1+2a)E_x^{n+3/4}(i+\tfrac{1}{2},j,k)-aE_x^{n+3/4}(i+\tfrac{1}{2},j+1,k) = \\ &= (1-2a)E_x^{n+1/4}(i+\tfrac{1}{2},j,k)+b\begin{pmatrix} H_z^{n+1/4}(i+\tfrac{1}{2},j+\tfrac{1}{2},k) \\ -H_z^{n+1/4}(i+\tfrac{1}{2},j-\tfrac{1}{2},k)\end{pmatrix}+a\begin{pmatrix} E_x^{n+1/4}(i+\tfrac{1}{2},j+1,k) \\ +E_x^{n+1/4}(i+\tfrac{1}{2},j-1,k)\end{pmatrix} \end{aligned} \tag{1.58}$$

where

$$a = \frac{\Delta t^2}{4\varepsilon\mu\Delta y^2} \text{ and } b = \frac{\Delta t}{\varepsilon\Delta y}. \tag{1.59}$$

Equation (1.58) represents a matrix equation and is tri-diagonal in nature. Its solution determines $E_x^{n+3/4}$. The size of the matrix is determined by N_y, the number of nodes along the y-axis. The matrix size being large, indirect matrix solution techniques are employed. An alternate-direct implicit Douglas-Gunn algorithm has been used by Sun and Trueman [36]. Yang et al. used a biconjugate-gradient (BCG) algorithm with symmetric successive over-relaxation (SSOR) as a pre-conditioner to speed up the BCG algorithm [37].

The field $E_x^{n+3/4}$ obtained above may be used to explicitly update $H_z^{n+3/4}$ through Equation (1.55b) according to

$$\begin{aligned} &H_z^{n+3/4}(i+\tfrac{1}{2},j+\tfrac{1}{2},k) \\ &\quad = H_z^{n+1/4}(i+\tfrac{1}{2},j+\tfrac{1}{2},k)+f\begin{pmatrix} E_x^{n+1/4}(i+\tfrac{1}{2},j+1,k)-E_x^{n+1/4}(i+\tfrac{1}{2},j,k)+ \\ E_x^{n+3/4}(i+\tfrac{1}{2},j+1,k)-E_x^{n+3/4}(i+\tfrac{1}{2},j,k)\end{pmatrix} \end{aligned} \tag{1.60}$$

where

$$f = \frac{\Delta t}{2\mu\Delta y} \tag{1.61}$$

We can similarly solve for $E_y^{n+3/4}$ and $E_z^{n+3/4}$ and update other H-field components, e.g.

$$H_x^{n+3/4}(i,j+\tfrac{1}{2},k+\tfrac{1}{2}) = H_x^{n+1/4}(i,j+\tfrac{1}{2},k+\tfrac{1}{2}) + g\begin{pmatrix} E_y^{n+1/4}(i,j+\frac{1}{2},k+1) - E_y^{n+1/4}(i,j+\frac{1}{2},k) + \\ E_y^{n+3/4}(i,j+\frac{1}{2},k+1) - E_y^{n+3/4}(i,j+\frac{1}{2},k) \end{pmatrix} \tag{1.62}$$

where

$$g = \frac{\Delta t}{2\mu\Delta z}. \tag{1.63}$$

Similarly, (1.56) may be discretized and solved to update the field components. This completes one cycle of time step updation.

The field updating procedure described above assumes that the initial field values are available at $t = (1/4)\Delta t$. Tan proposes the following input processing from $t = 0$ to $t = (1/4)\Delta t$ [38]

$$\left([I] - \frac{\Delta t}{4}[B]\right)\mathbf{u}^{1/4} = \left([I] + \frac{\Delta t}{4}[B]\right)\mathbf{u}^{0} \tag{1.64}$$

Use of Equation (1.49b) for matrix B results in

$$E_x^{1/4} - \frac{\Delta t^2}{16\mu\varepsilon}\frac{\partial^2 E_x^{1/4}}{\partial z^2} = E_x^0 + \frac{\Delta t^2}{16\mu\varepsilon}\frac{\partial^2 E_x^0}{\partial z^2} - \frac{\Delta t}{2\varepsilon}\frac{\partial H_y^0}{\partial z} \tag{1.65a}$$

$$H_y^{1/4} = H_y^0 - \frac{\Delta t}{4\mu}\left(\frac{\partial E_x^0}{\partial z} + \frac{\partial E_x^{1/4}}{\partial z}\right) \tag{1.65b}$$

While the implementation of Equation (1.65a) requires the solution of a matrix equation similar to that for $E_x^{n+3/4}$ and described earlier, the update for $H_y^{1/4}$is explicit. Discretizing Equation (1.65) results in

$$\begin{aligned} &-pE_x^{1/4}(i+\tfrac{1}{2},j,k-1) + (1+2p)E_x^{1/4}(i+\tfrac{1}{2},j,k) - pE_x^{1/4}(i+\tfrac{1}{2},j,k+1) = \\ &= (1-2p)E_x^0(i+\tfrac{1}{2},j,k) + p\begin{pmatrix} E_x^0(i+\frac{1}{2},j,k+1) + \\ E_x^0(i+\frac{1}{2},j,k11) \end{pmatrix} - q\begin{pmatrix} H_y^0(i+\frac{1}{2},j,k+\frac{1}{2}) - \\ H_y^0(i+\frac{1}{2},j,k-\frac{1}{2}) \end{pmatrix} \end{aligned} \tag{1.66a}$$

$$H_y^{1/4}(i+\tfrac{1}{2},j,k+\tfrac{1}{2}) = H_y^0(i+\tfrac{1}{2},j,k+\tfrac{1}{2}) + s\begin{pmatrix} E_x^0(i+\frac{1}{2},j,k+1) - E_x^0(i+\frac{1}{2},j,k) + \\ E_x^{1/4}(i+\frac{1}{2},j,k+1) - E_x^{1/4}(i+\frac{1}{2},j,k) \end{pmatrix} \quad (1.66b)$$

where

$$p = \frac{\Delta t^2}{16\varepsilon\mu\Delta z^2}, \quad q = \frac{\Delta t}{2\varepsilon\Delta z} \text{ and } s = \frac{\Delta t}{4\mu\Delta z} \quad (1.67)$$

The following transformation is recommended for output processing of data from $\mathbf{F}^{n+5/4}$ to $\mathbf{F}^{n+1}$ [38]

$$\left([I] + \frac{\Delta t}{4}[B]\right)\mathbf{F}^{n+1} = \left([I] - \frac{\Delta t}{4}[B]\right)\mathbf{F}^{n+5/4} \quad (1.68)$$

The increased efficiency of LOD-FDTD compared to ADI-FDTD is due to the reduced number of arithmetic operations on the RHS of Equation (1.53) [35]. The number of arithmetic operations for the LOD and ADI schemes are compared in Table 1.1 [[35],Table 1].

Table 1.1 Comparison between ADI and LOD-FDTD schemes for the number of arithmetical operations

Arithmetical operations		ADI	LOD
Implicit	M/D	18	18
	A/S	48	24
Explicit	M/D	12	6
	A/S	24	24
Total	M/D	30	24
	A/S	72	48

Source: Reproduced by permission of ©2007 IEEE, Table 1 of [35].

Note: *M = multiplication, D = division, A = addition and S = subtraction.

It is observed in [38] that the various implicit FDTD schemes have similar updating structures, and it is possible to improve their efficiency using a general procedure. The approach devised is to express these algorithms in a form so that the RHS of transformations e.g. (1.54) should consist of least number of terms and should be free from the matrix operator. Auxiliary variables are introduced for this purpose. For the LOD-FDTD described above we may define the auxiliary variables as [38]

$$F^{n+3/4} = H^{n+3/4} - F^{n+1/4} \quad \text{and} \quad F^{n+5/4} = H^{n+5/4} - F^{n+3/4} \quad (1.69)$$

The expressions (1.54) then transform to

$$\left(\frac{1}{2}[I] - \frac{\Delta t}{4}[A]\right)H^{n+3/4} = F^{n+1/4} \quad \left(\frac{1}{2}[I] - \frac{\Delta t}{4}[B]\right)H^{n+5/4} = F^{n+3/4} \quad (1.70)$$

This LOD algorithm is more efficient than Equation (1.54) because the RHS of Equation (1.70) is free from matrix operators. The efficiency of the modified algorithm is found to be 1.83 times that of the ADI-FDTD algorithm of Equation (1.53) [38].

The LOD-FDTD algorithm for circularly symmetric geometries has been reported. The improvement in efficiency compared to ADI-FDTD has been reported to be about 40% [39]. Extension of LOD-FDTD method to dispersive media has been reported by Shibayama et al. [40]. The improvement in efficiency is found to be about 30% compared to FDTD(2,2).

1.6.1 PML Absorbing Boundary Condition for LOD-FDTD

For the use of LOD-FDTD to antennas, the electromagnetic geometry must be terminated with reflectionless boundaries. Split field and unsplit field PML have been formulated for LOD-FDTD in [41] and [42], respectively. The reflection coefficient of the order of -75 dB has been reported for the split-field PML in the context of a two-dimensional TE case [41]. It has been observed that unsplit field non-dispersive PML gives reflection of the order of -17 dB for $q = 2$, and -12 dB for $q = 4$. However, complex envelope unsplit field dispersive PML gives better performance, -33 dB for $q = 2$ and -25 dB for $q = 4$ [42]. Convolutional PML (CPML) has been found to give better performance than other forms of PML for LOD-FDTD [43]. It is found that CPML gives lower reflection by about 16 dB compared to FDTD-PML for $q = 1$. This is shown in Figure 1.14 for 8 layers of CPML. The reflection from CPML is found to decrease with increase in q number due to the increased value of $E_{ref\ \max}$ [43]. This is shown in Figure 1.15.

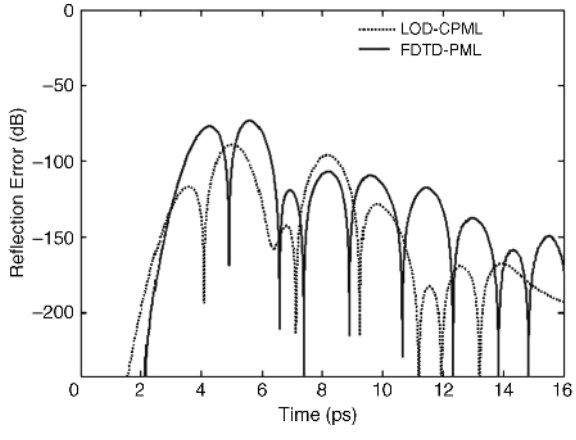

Figure 1.14 Comparison of reflection error from LOD-CPML and FDTD-PML for $q = 1$. Reproduced by permission of ©2007 IEEE, Figure 2 of [43]

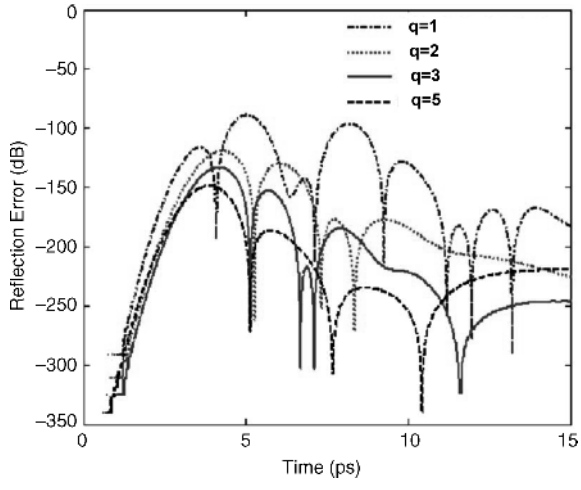

Figure 1.15 Comparison of reflection error from LOD-CPML for four values of q. Reproduced by permission of ©2007 IEEE, Figure 3 of [43]

1.7 Robustness of Printed Patch Antennas

The printed antennas are likely to get damaged when they brush against some hard object during use. When used as an RFID antenna, the environment is expected to be relatively harsh. The damage may occur to the top metallization, produce voids in dielectric subatrate, etc. In addition, the substrate may have non-uniform thickness and dielectric constant. The effect of these degradations on the resonant frequency of patch antennas has been studied analytically and verified numerically [44]. The analysis may be carried out based on perturbation technique. It has been found that the robustness of microstrip antennas is directly related to the substrate damage volume and position. The change in resonance frequency of the antenna is directly proportional to the volume and the change in permittivity of the defect. Small damage to the patch metallization alone does not affect return loss.

1.8 Thin Dielectric Approximation

The printed flat antennas on dielectric films are being used increasingly because they can be made into complicated shapes. Often the film is very thin and is less than one cell along the thickness. Use of uniform cell size is not advisable because of too much demand on computer resources. The other alternatives are non-uniform grid, or local refinement in the region, or sub-cell algorithm. Another alternative is to model the field distribution in the film region using quasi-static approximation. The geometry of a metal strip on a thin dielectric film is shown in Figure 1.16. Using the sub-cell approach for the tangential fields E_x and E_y, one needs to replace ε and σ in (1.4) by their average values defined as

$$\varepsilon_{avg} = \frac{\varepsilon_0(\Delta z - d) + \varepsilon_r d}{\Delta z} \qquad \sigma_{avg} = \frac{\sigma d}{\Delta z} \tag{1.71}$$

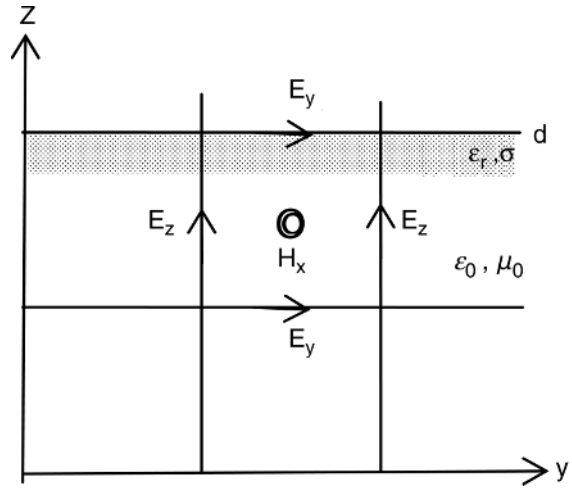

Figure 1.16 Thin dielectric film in a FDTD cell. Reproduced by permission of ©2004 IEEE [45]

where d is the film thickness, Δz is cell size along the film thickness, ε_r and σ are electrical parameters of the film. The field E_z near the strip edge is dominated by the static field, and may be included in the FDTD algorithm as described in [45, 46].

1.9 Modeling of PEC and PMC for Irregular Geometries

The PEC or PMC boundaries may not conform in places to the grid employed for the FDTD analysis of complex geometrical shapes. The modifications for such cases include conformal FDTD (C-FDTD) method [47], contour-path FDTD (CP-FDTD) method [48], sub-cell models [49], etc. These methods may require changes in existing source codes, grid, and time step. Sometimes, staircase approximation of the geometry is employed. A new method has been suggested in [50] and does not involve disturbing the original grid. The method involves extrapolation of (tangential) field values from the adjacent internal node to obtain exterior field values so that the perfect boundary condition in between is satisfied. The new method can be applied to model parallel, slanted, and curved walls in the existing FDTD grid [50]. Time step reduction is not necessary.

To illustrate this method we consider a rectangular resonator whose cross-section in the x–y plane is shown in Figure 1.17. The geometry is deliberately displaced along the y-axis so that the PEC on the LHS and RHS do not coincide but are parallel to the existing grid. Let the displacement with respect to the grid be $\xi\Delta y$, $0 < \xi < 1$. The PEC walls are now located off-grid. The field values at the LHS PEC wall at $y = \xi\Delta y$ is modeled in a linear fashion from the values at nearby node at $y = \Delta y$. Let us denote the tangential component of electric field $F(\Delta y) = f_1$. Assuming linear variation of field between adjacent layers of nodes at $y = \Delta y$ and $y = \xi\Delta y$, we can write[50]

$$F(\Delta y) = f_1 = a\Delta y + b \tag{1.72a}$$

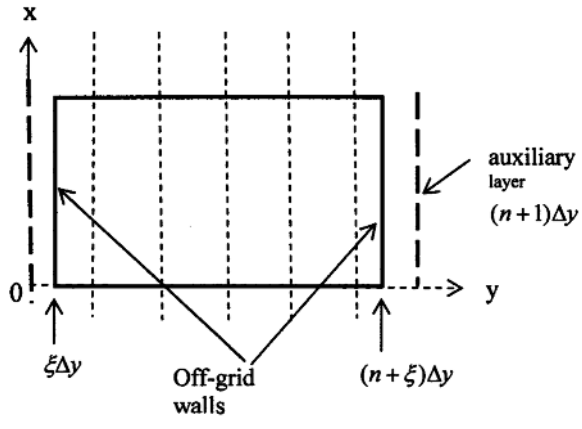

Figure 1.17 Cross-section of a rectangular cavity in the *x*-*y* plane. The cavity is offset from the grid by $\xi\Delta y$. Reproduced by permission of ©2005 IEEE, Figure 1 of [50]

$$F(\xi\Delta y) = 0 = a\xi\Delta y + b \quad \text{due to PEC} \tag{1.72b}$$

Eliminating a and b gives for the field in the vicinity of PEC boundary as

$$F(y) = \frac{f_1}{1-\xi}\left(\frac{y}{\Delta y} - \xi\right) \tag{1.73}$$

Application of (1.73) to the layer at $y = 0$, left of PEC, gives

$$F(0) = f_0 = f_1\left(\frac{\xi}{\xi - 1}\right), \quad \text{for } \xi \leq \xi_{\max} \tag{1.74}$$

Obviously, this layer is external to the computational domain.

Similarly, the PEC boundary condition on the RHS at $y = (n+\xi)\Delta y$ can be satisfied from the known field values at $y = n\Delta y$. The resulting expression for f_{n+1} is given by

$$F((n+1)\Delta y) = f_{n+1} = \left(\frac{\xi - 1}{\xi}\right) f_n \quad \text{for } \xi \geq 1 - \xi_{\max} \tag{1.75}$$

The extrapolation of internal field values to the adjacent layers beyond the perfect boundaries has a limitation on the offset ξ called $\xi_{\max}$ for (1.74) and $\xi_{\max} = 1 - \xi_{\max}$ for (1.75). The coefficient in these expressions approaches infinity as $\xi \to 1$ and gives rise to instability in the algorithm. The permissible value of $\xi_{\max}$ is given by [50]

$$\xi_{\max} = 0.643 + 0.584\sqrt{1 - 1.01q} \tag{1.76}$$

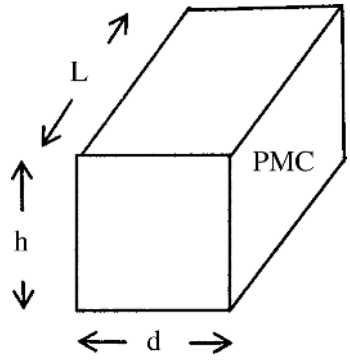

Figure 1.18 A rectangular cavity with PMC at the right-hand side

where q is the Courant number. For $0.866 \leq q \leq 0.98625$ the corresponding range of $\xi_{\max}$ is $0.85 \geq \xi_{\max} \geq 0.7$. Offsets $\xi > \xi_{\max}$ are also discussed in [50].

The simple approach for Dirichlet boundary condition has been extended to the off-grid Neumann boundary condition, slanted PEC walls and curved PEC walls. The above approach is verified by computing the resonant frequencies of a rectanglar cavity with PEC at one end and PMC at the other end, as shown in Figure 1.18. The cavity dimensions are: $h = 10$ mm, $d = 10$ mm, and $L = 30$ mm; the step sizes used are: $\Delta x = \Delta y = \Delta z = 1$ mm and $q = 0.88$. Comparison of the computed and analytical resonant frequencies are given in Table 1.2 for $\xi = 0.15$ [50]. The accuracy is fairly good.

Table 1.2 Relative error of the resonant frequencies of a rectangular cavity with off-grid (left) PEC and (right) PMC walls, $\xi = 0.15$

Analytical (GHz)	Calculated (GHz)	Error (%)
$f_{011} = 9.007642$	9.00277	0.054
$f_{012} = 12.491352$	12.48096	0.083
$f_{110} = 16.758909$	16.72183	0.221
$f_{111} = 17.487894$	17.45512	0.182

Source: Reproduced by permission of ©2005 IEEE, Table II of [50].

References

1. R. Garg, P. Bhartia, I. Bahl, and A. Ittipiboon, *Microstrip Antenna Design Handbook*, Artech House, Boston, 2001.
2. A. Taflove, and S.C. Hagness, *Computational Electromagnetics: The Finite-Difference Time Domain Method*, 3rd edition, Artech House, Boston, 2005.
3. K.S. Yee, "Numerical solution of initial boundary value problems involving Maxwell's equations in isotropic media," *IEEE Trans. Antennas Propagat.*, vol. AP-14, pp. 302–307, 1966.
4. A. P. Zhao, "Rigorous analysis of the influence of the aspect ratio of the Yee's unit cell on the numerical dispersion property of the 2-D and 3-D FDTD methods," *IEEE Trans. Antennas Propagat.*, vol. 52, no. 7, pp. 1633–1637, July. 2004.
5. S.V. Georgakopoulos, C.R. Birtcher, C.A. Balanis, and R.A. Renaut, "Higher-order finite-difference schemes for electromagnetic radiation, scattering, and penetration, Part I: Theory," *IEEE Antenna Propagate. Mag.*, vol. 44, pp. 134–142, Feb. 2002.

6. Z. Huang, G. Pan, and R. Diaz, "A hybrid ADI and SBTD scheme for unconditionally stable time-domain solutions of Maxwell's equations," *IEEE Trans. Packag.*, vol. 31, no. 1, pp. 219–226, 2008.
7. T. Dogaru, and L. Carin, "Multiresolution time-domain using CDF biorthogonal wavelets," *IEEE Trans. Microw. Theory Tech.*, vol. 49, no. 5, pp. 902–912, 2001.
8. S. Ogurtsov, and P. Guangwen, "An updated review of general dispersion relation for conditionally and unconditionally stable FDTD algorithms", *IEEE Trans. Antennas Propagat.*, vol. 56, no. 8, Part 2, pp. 2572–2583, Aug. 2008.
9. S. Ogurtsov, and S. V. Georgakopoulos, "FDTD schemes with minimal numerical dispersion," *IEEE Trans. Adv. Packag.*, vol. 32, no. 1, pp. 199–204, Feb. 2009.
10. C. D. Moss, F. L. Teixeira, and J. A. Kong, "Analysis and compensation of numerical dispersion in the FDTD method for layered, anisotropic media," *IEEE Trans. Antennas Propagat.*, vol. 50, no. 9, pp. 1174–1184, Sept. 2002.
11. A. P. Zhao, J. Juntunen, and A. V. Raisanen, "An efficient FDTD algorithm for the analysis of microstrip patch antennas printed on a general anisotropic dielectric substrate," *IEEE Trans. Microw. Theory Tech.*, vol. 47, no. 7, pp. 1142–1146, 1999.
12. R. M. Makinen, H. De Gersem, T. Weiland, and M. A. Kivikoski, "Modeling of lossy curved surfaces in 3-D FIT/ FDTD techniques," *IEEE Trans. Antennas Propagat.*, vol. 54, no. 11, pp. 3490–3498, 2006.
13. M. K. Karkkainen, and S. A. Tretyakov, "Finite-difference time-domain model of interfaces with metals and semiconductors based on a higher order surface impedance boundary condition," *IEEE Trans. Antennas Propagat.*, vol. 51, no. 9, pp. 2448–2455, 2003.
14. S. Ogurtsov, G. Pan, and R. Diaz, "Examination, clarification, and simplification of stability and dispersion analysis for ADI-FDTD and CNSS-FDTD schemes," *IEEE Trans. Antennas Propagat.*, vol. 55, no. 12, pp. 3595–3602, Dec. 2007.
15. T. K. Sarkar, and O. Pereira, "Using the matrix pencil method to estimate the parameters of a sum of complex exponentials," *IEEE Trans. Antennas Propagat.*, vol. 37, no. 1, pp. 48–55, Feb. 1995.
16. L. Qing, X. Xiaowen, and H. Mang, "Analysis of a probe-fed cylindrical conformal microstrip patch antenna using the conformal FDTD algorithm," *IEEE 2007 Int. Sym. on Microwave, Ant., Propag. and EMC Tech. for Wireless Commun.*, pp. 876–879, 2007.
17. B. Enquist, and A. Majda, "Absorbing boundary conditions for the numerical simulation of waves," *Mathematics of Computation*, vol. 31, pp. 629–651, 1977.
18. G. Mur, "Absorbing boundary conditions for the finite difference approximation of the time domain electromagnetic field equations," *IEEE Trans., EMC-23*, pp. 377–382, 1981.
19. R. L. Higdon, "Absorbing boundary conditions for difference approximations to the multidimensional wave equation," *Math. Comput.*, vol. 47, pp. 437–459, 1986.
20. Z. P. Liao, H. L. Wong, B.-P. Yang, and Y.-F. Yuan, "A transmitting boundary for transient wave analysis," *Scientia Sinica*, Ser. A. vol. 27, pp. 1063–1076, Oct. 1984.
21. F. Costen, "Analysis and improvement of Liao ABC for FDTD," *IEEE APS-2003*, pp. 341–344, 2003.
22. M. K. Karkkainen, and S. A. Tretyakov, "A class of analytical absorbing boundary conditions originating from the exact surface impedance boundary condition," *IEEE Trans. Microwave Theory Tech.*, vol. 51, pp. 560–563, 2003.
23. S. Tretyakov, *Analytical Modeling in Applied Electromagnetics*, Artech House, Boston, 2003.
24. N. V. Kantartzis, and T. D. Tsiboukis, "A comparative study of the Berenger perfectly matched layer, the superabsorption technique and several higher-order ABC's for the FDTD algorithm in two- and three-dimensional problems," *IEEE Trans. Mag.*, vol. 33, pp. 1460–1463, March 1997.
25. R. Hallond, and J. W. Williams, "Total field versus scattered field finite difference codes: a comparative assessment," *IEEE Trans. Nuclear Science*, vol. NS-30, pp. 4583–4587, 1983.
26. J. P. Berenger, "A perfectly matched layer for the absorption of electromagnetic waves," *J. Computational Physics*, vol. 114, pp. 185–200, 1994.
27. W. C. Chew, J. Jin, E. Michielssen, and J. Song, *Fast and Efficient Algorithms in Computational Electromagnetics*, Artech House, Boston, 2001.
28. S. D. Gedney, "An anisotropic perfectly matched layer absorbing medium for the truncation of FDTD lattices," *IEEE Trans. Antennas Propagat.*, vol. AP-44, pp. 1630–1639, 1996.
29. J. A. Kong, *Electromagnetic Wave Theory*, 2nd edition, John Wiley& Sons, Ltd, New York, 1990.
30. Z. H. Huang, and G. W. Pan, "Universally applicable uniaxial perfect matched layer formulation for explicit and implicit finite difference time domain algorithms", *IET Microw. Antennas Propag.*, vol. 2, no. 7, pp. 668–676, 2008.

31. D. M. Sullivan, "An unsplit step 3-D PML for use with the FDTD method," *IEEE Microw. Guided Wave Lett.*, vol. 7, no. 7, pp. 184–186, 1997.
32. A. P. Zhao, "Uniaxial perfectly matched layer media for an unconditionally stable 3-D ADI-FDTD method," *IEEE Microw. Wireless Compon., Lett.*, vol. 12, no. 12, pp. 497–499, 2002.
33. T. Namiki, "A new FDTD algorithm based on alternating-direction implicit method," *IEEE Trans. Microwave Theory Tech.*, vol. 47, pp. 2003–2007, 1999.
34. J. Shibayama, M. Muraki, J. Yamauchi, and H. Nakano, "Efficient implicit FDTD algorithm based on locally one-dimensional scheme," *Electron. Lett.*, vol. 41, no. 19, pp. 1046–1047, 2005.
35. E. L. Tan, "Unconditionally stable LOD-FDTD method for 3-D Maxwell's equations," *IEEE Microw. Wireless Compon., Lett.*, vol. 17, no. 2, pp. 85–87, 2007.
36. G. Sun, and C. W. Trueman, "Unconditionally stable Crank-Nicolson scheme for solving two-dimensional Maxwell's equations," *Electron. Lett.*, vol. 39, pp. 595–597, April 3, 2003.
37. Y. Yang, R. S. Chen, D. X. Wang, and E. K. N. Yung, "Unconditionally stable Crank-Nicolson finite-difference time-domain method for simulation of three-dimensional microwave circuits," *IET Microw. Antennas Propag.*, vol. 4, pp. 937–942, 2007.
38. E. L. Tan, "Fundamental schemes for efficient unconditionally stable implicit finite-difference time-domain methods," *IEEE Trans. Antennas Propag.*, vol. 56, no. 1, pp. 170–177, 2008.
39. J. Shibayama, B. Murakami, J. Yamauchi, and H. Nakano, "LOD-BOR-FDTD algorithm for efficient analysis of circularly symmetric structures," *IEEE Microw. Wireless Compon., Lett.*, vol. 19, no. 2, pp. 56–58, 2009.
40. J. Shibayama, R. Takahashi, J. Yamauchi, and H. Nakano, "Frequency-dependent implementations for dispersive media," *Electron., Lett.*, vol. 42, no. 19, pp. 1084–1085, 2006.
41. V. E. Nascimento, B. H. Borges, and F. L. Teixeira, "Split-field PML implementations for the unconditionally stable LOD-FDTD method," *IEEE Microw. Wireless Comp., Lett.*, vol. 16, no. 7, pp. 398–400, 2006.
42. O. Ramadan, "Unsplit field implicit PML algorithm for complex envelope dispersive LOD-FDTD simulations," *Electron., Lett.*, vol. 43, no. 5, pp. 17–18, 2007.
43. I. Ahmed, E. Li, and K. Krohne, "Convolutional perfectly matched layer for an unconditionally stable LOD-FDTd method," *IEEE Microw. Wireless Compon., Lett.*, vol. 17, no. 12, pp. 816–818, 2007.
44. T. Olsson, J. Siden, M. Hjelm, and H.-E. Nilsson, "Robustness of printed patch antennas," *IEEE Trans. Antennas Propagat.*, vol. 55, pp. 2709–2717, Oct. 2007.
45. T. Arima, T. Uno, and M. Takahashi, "FDTD analysis of printed antenna on thin dielectric sheet including quasi-static approximation," *2004 IEEE APS Digest*, pp. 1022–1025.
46. T. Arima, T. Uno, and M. Takahashi, "Improvement of FDTD accuracy for analyzing printed antennas by using quasi-static approximation," *2003 IEEE APS Digest*, vol. 3, pp. 784–787, 2003.
47. S. Dey, and R. Mittra, "A locally conformal finite-difference time-domain (FDTD) algorithm for modeling three-dimensional perfectly conducting objects," *IEEE Microw. Guided Wave Lett.*, vol. 7, no. 9, pp. 273–275, 1997.
48. C. J. Railton, I. J. Craddock, and J. Achneider, "The analysis of general two-dimensional PEC structures using a modified CPFDTD algorithm," *IEEE Trans. Microwave Theory Tech.*, vol. 44, no. 10, pp. 1728–1733, 1996.
49. J. Anderson, M. Okoniewski, and S. S. Stuchly, "Subcell treatment of 90 degree metal corners in FDTD," *Electron., Lett.*, vol. 31, pp. 2159–2160, 1995.
50. Y. S. Rickard, and N. K. Nikolova, "Off-grid perfect boundary conditions for the FDTD method," *IEEE Trans. Microwave Theory Tech.*, vol. 53, no. 7, pp. 2274–2283, 2005.